Journal of
Nanoscience and Nanotechnology
Vol. 11, 1–7, 2011

Nano and Micro Reoriented Domains and Their Relation with the Crystal Structure in the New $Fe_{1.5}Zn_{1.5}B_7O_{13}Cl$ Boracite

S. Ulloa-Godínez[1,5], A. Barrera[2], I. Rosales[3], L. Bucio[3], F. F. Castillon[4], M. H. Farias[4], J. M. Siqueiros[4], and J. Campa-Molina[1,*]

[1] *Centro Universitario de Ciencias Exactas e Ingeniería, Universidad de Guadalajara, Laboratorio de Materiales Avanzados del Departamento de Electrónica. Av. Revolución No.1500, Módulo O, Planta baja, S.R. C.P. 44840, Guadalajara, Jalisco, México*
[2] *Centro Universitario de la Ciénega, Universidad de Guadalajara, Laboratorio de Materiales, Av. Universidad No. 1115, Colonia Linda Vista, C.P. 47840, Ocotlán, Jalisco, México*
[3] *Instituto de Física, Universidad Nacional Autónoma de México, Apartado Postal 20-364, C.P. 01000 México, D. F., México*
[4] *Centro de Nanociencias y Nanotecnología, Universidad Nacional Autónoma de México, Apdo. Postal 356, C.P. 22800, Ensenada, Baja California, México*
[5] *Facultad de Ingeniería, Universidad Autónoma de Baja California, Blvd. Benito Juarez s/n col. Insurgentes, Mexicali, Baja California, México*

New iron–zinc chlorine single crystals of $Fe_{1.5}Zn_{1.5}B_7O_{13}Cl$ boracite were grown by chemical transport reactions in closed quartz ampoules, at a temperature of 1173 K. The crystal structure was characterized by X-ray powder diffraction (XRD) using the Rietveld refinement method and belongs to the trigonal/rombohedral system with space group *R*3*c* (No. 161). The cell parameters were $a = 8.5726(1)$ Å, $c = 21.0116(4)$ Å, $V = 1337.26(3)$ Å^3 and $Z = 6$. The refinement successfully proceeded and ended with sound merit figure values $\chi^2 = 2.25$, $R_B = 6.12\%$. Chemical analysis was performed with X-ray energy dispersive spectroscopy (EDS) and X-ray fluorescence (XRF). Ferroelectric nano and micro reoriented domains were found in this material using polarizing optical microscopy (PLM), scanning electron microscopy (SEM) and transmission electron microscopy (TEM). The examination by TEM showed that in the trigonal/rombohedral system of $Fe_{1.5}Zn_{1.5}B_7O_{13}Cl$ nanodomain structures exist. Thin (50–100 nm) mostly planar domains parallel to (100) were frequently observed in $Fe_{1.5}Zn_{1.5}B_7O_{13}Cl$ boracite.

Keywords: Structural Characterization, Domain Structure, New Boracite.

RESEARCH ARTICLE

1. INTRODUCTION

Natural and synthetic boracites have attracted the attention of researchers since the early times of crystallography, when Haüy observed pyroelectricity for the first time in natural boracites,[1] a phenomenon which later was studied in detail by Hankel et al.[2] The mineral boracite $Mg_3B_7O_{13}Cl$, which provides the name of this large family, is currently found in bedded sedimentary deposits of anhydrite, gypsum and halite.[1] Only other four natural boracites are known: ericaite (Fe, Mg)$_3B_7O_{13}Cl$, named in 1950 for its purple colour (Erica is the heather genius[1]); chambersite $Mn_3B_7O_{13}Cl$, named in 1962 after a locality in the state of Texas;[3] congolite $Fe_3B_7O_{13}Cl$, named in 1972 after the country of origin[4] and trembathite (Mg, Fe)$_3B_7O_{13}Cl$, named in 1992 in honour of Lowell T. Trembath, a canadian mineralogist.[4] Ericaite and trembathite are natural mixed boracites, which have been taken as motivation in this investigation to synthesize other types of mixed boracites. The synthesis of mixed boracites can provide around 300 new combinations. The idea of synthesizing the mixed of $Fe_{1.5}Zn_{1.5}B_7O_{13}Cl$ boracites, it is in order to improving their physical properties, when combining them those of both materials. In subsequent works we will report the studies carried out on the $Fe_{1.5}Zn_{1.5}B_7O_{13}Cl$ boracites with regard to their primary properties, i.e., ferroelectricity, ferroelasticity, ferromagnetism and ferrotoroidicity.[5]

In a previous work on the domain structure of $Mn_3B_7O_{13}X$ and $Zn_3B_7O_{13}X$ (where X = Cl, Br or I) boracites,[6–8] a detailed description was presented of the

*Author to whom correspondence should be addressed.

ferroic phase transitions displayed by these materials, which give place to a classification scheme based on the tensor properties of the twin domains. In particular, $Zn_3B_7O_{13}X$ boracites transform from a cubic high temperature phase (point group $\bar{4}3m$) to a 'fully ferroelectric/fully ferroelastic' phase (for general nomenclature see Aizu, 1970; Schmid, 1992)[9,10] with point group mm2.[11] The transition temperature (T_c) follows the order Cl → Br → I ($T_c = 786$ K for $Zn_3B_7O_{13}Cl$, $T_c = 585$ K for $Zn_3B_7O_{13}Br$ and $T_c = 319$ K for $Zn_3B_7O_{13}I$). Additional phase transitions have been observed in $Zn_3B_7O_{13}Cl$, from the orthorhombic phase to a monoclinic phase with point group m ($T_c = 567$ K),[11] and then to a trigonal phase with point group 3m at 480 K.[12] Phase transitions accompanied by a change of the point-group symmetry are generally called ferroic.[13] A ferroic crystal contains two or more possible orientation states or domains; under a suitably chosen driving force the domain walls (i.e., the intermediate regions between domains) move, switching the crystal from one domain to another.[9] The formation of domains is a normal phenomenon occurring during nondestructive ferroic phase transitions involving symmetry reduction, usually upon cooling from the high temperature phase. In such a case the twinning laws of the ferroic phase, i.e., the symmetry operations to transform one domain into all others, are given by the symmetry elements lost during the transition.[10,14–16] In this sense, synthetic $Zn_3B_7O_{13}X$ boracite crystals at temperatures lower than the transition temperature, T_c, are characteristically twinned. The study of domain structures is important for understanding properties of ferroelectric materials because their properties are to a large extent determined by domain structures.[11,17] In particular, on the one hand they deteriorate pyroelectric figures of merit by decreasing the values of odd-rank tensors and increasing noise, but on the other hand they enhance electrical, mechanical and piezoelectric susceptibilities due to domain walls.[15] To our knowledge, very few attempts have been made to correlate physical properties of boracites to their domain structures.[18,19] The reason could be that for the experimental study of a ferroelectric material the interest usually focuses on single crystals which are both single domain electrically and untwinned crystallographically, so the starting point is to apply a poling process to the sample, thus 'destroying' its initial domain structure.

Nowadays, boracites have received special attention because of their unusual physical properties, which make them have potential applications: an optic stopper due to the modification in birefringence produced by the application of a mechanical strain, electric field, electron beam and/or temperature change;[20] ferroelectric nonvolatile memory (ferroelectric random access memory, or FRAM) because of the reorientation of its ferroelectric domains;[21] and infrared (IR) detection due to the intrinsic pyroelectricity of the boracites.[6,22] One characteristic that makes these boracites unique is the ferroelectricity phenomenon (domain reorientation) which can be observed using almost any microscopy technique, while, in most of the ferroelectric compounds, the ferroelectricity is confirmed just with a hysteresis cycle.[6,22]

This paper reports the synthesis of a new iron-zinc chlorine boracite $Fe_{1.5}Zn_{1.5}B_7O_{13}Cl$ grown by chemical transport reaction in closed quartz ampoules at 1173 K. The crystal structure was characterized by X-ray powder diffraction (XRD) applying the Rietveld refinement method. Also, ferroelectric nano and micro reoriented domains were found in this material using polarizing optical microscopy (PLM), scanning (SEM) and transmission electron microscopy (TEM).

2. EXPERIMENTAL DETAILS

To perform the method of Schmid[23] for sample preparation of crystalline materials, the reactants were placed in three fused silica crucibles, vertically placed and spatially separated by quartz rods in the following order starting from the bottom: 1.7 g of B_2O_3 (which was obtained by dehydrating H_3BO_3) was placed in the first crucible; 0.5 g of each one of both metal oxides (ZnO and FeO) in the second crucible; and finally 0.8 g of each one of both divalent metal halides ($FeCl_2$ and $ZnCl_2$) in the third crucible. Chemical transport reactions were carried out by heating the ampoule in a furnace according to the following heating steps: 1173 K over a period of 50 hours and 913 K over a period of 20 hours. After this procedure $Fe_{1.5}Zn_{1.5}B_7O_{13}Cl$ mixed boracite single crystals were grown, clear yellow in colour, which formed mostly on the lower crucible. Additionally, some smaller crystals up to 1 mm in size grew on the bottom of the quartz ampoule.

X-ray powder diffraction patterns (XRD) were recorded, at room temperature, in a Bruker Advance D8 diffractometer with a vertical goniometer. A fixed diffracted beam graphite monochromator and a lynx-eye detector were used to measure the diffracted beam of X-rays produced in a CuKα anode operating at 40 kV and 25 mA. The 2θ-range covered was from 10° to 110° with 0.019° steps.

Energy dispersive spectrometry (EDS) were carried out under a low vacuum scanning electron microscopy, JEOL JSM-5600LV. A small crystallite was placed on a carbon double sided tape fixed to an aluminum sample holder inside the microscope. The EDS spectrum was taken at different zones in the sample.

X-ray Fluorescence (XRF) was used to perform the ratio between Fe and Zn in the $Fe_{1.5}Zn_{1.5}B_7O_{13}Cl$ mixed boracite. A small crystallite was irradiated using the 'SANDRA' system developed at Instituto de Fisica, UNAM, equipped with a 75 W Mo X-ray tube (50 kV, 1.5 mA, XTF5011 model from Oxford Instruments) and AmpTeK Si-Pin detector. The system was calibrated using reference standard materials from NIST (SRM 2711).

For performing PLM and SEM measurements, platelets from an as-grown crystal parallel to a naturally formed (111) facet of $Fe_{1.5}Zn_{1.5}B_7O_{13}Cl$ were cut. For PLM, the opposite surface of the specimen was polished to optical quality by using 0.7 μm grain size diamond paste. The surfaces of $Fe_{1.5}Zn_{1.5}B_7O_{13}Cl$ were not metallized. The typical sample thickness was 60 μm and the area ranged up to 0.0145 cm^2. The observed $Fe_{1.5}Zn_{1.5}B_7O_{13}Cl$ sample was freely mounted on the rotary stage of a polarizing light microscope (Leitz Ortoplan Pol). For SEM, the same sample was attached to a brass cylindrical holder with a carbon tape. The holder was mounted in a JEOL SEM 5200 microscope with a NORAN-EDX instrument for EDS measurements. For TEM, the sample was crushed in a mortar and suspended in alcohol. A drop of the solution was released on a specimen grid covered by a thin holey carbon film. Finally, for the analysis, the sample was mounted on the sample stage of a JEOL STEM 100-CX.

3. RESULTS AND DISCUSSION

3.1. Structural Characterization

The characterization of powdered $Fe_{1.5}Zn_{1.5}B_7O_{13}Cl$ mixed boracite by conventional X-ray powder diffraction data indicated the presence of a well crystallized phase showing reflections that matched with the isostructural phase trembathite $Mg_{1.56}Fe_{1.44}Mn_{0.02}B_7O_{13}Cl$ (PDF 01-089-6198) reported by Schindler and Hawthorne.[24] The starting structural parameters to perform a Rietveld refinement of the $Fe_{1.5}Zn_{1.5}B_7O_{13}Cl$ boracite were taken from the isostructural data reported for $Zn_3B_7O_{13}Cl$ (ICSD 55444) by Mao et al.[12] The FULLPROF program[25] was used for the refinement process. A pseudo-Voigt function modified by Thompson, Cox and Hastings[26] was chosen to generate the shape of the diffraction peaks. The following parameters were refined: zero point, scale factor, linear interpolation between 89 fixed points for the background, unit cell dimensions, half-width, pseudo-Voigt and asymmetry parameters for the peak shape; position and thermal isotropic factors. For the case of boron, the thermal isotropic factors were fixed to 0.24 Å,[2] which is a reasonable value for the boron atom and for obtaining a good refinement. The occupation factors for Fe and Zn atoms sharing the same position were fixed to the value of 0.5 for both atoms according to the results of chemical analysis (Fe/Zn ratio) obtained by EDS and X-ray fluorescence (XRF).

Rigid-body model with constrained generalized coordinates were defined in order to hold the positions of boron atoms at reasonable interatomic distances that typically would reach unacceptable values because of the weak scattering power for X-rays of boron. One rigid body group (RBG) containing the boron atoms was defined as illustrated in Figure 1. This RBG has its centre in O(1) atom. Then, eight atoms define the complete RGB (including the centre) and are labelled as B(1), B(2), B(3), O(1), O(2), O(3), O(4) and O(5). The positional parameters refined in a first step were limited by the symmetry allowed movements for the RBG as a whole. At the end of this step, $B(1)O_4$, $B(2)O_4$ tetrahedra, and $B(3)O_3$ triangle kept their interatomic angles and distances. In a second and final

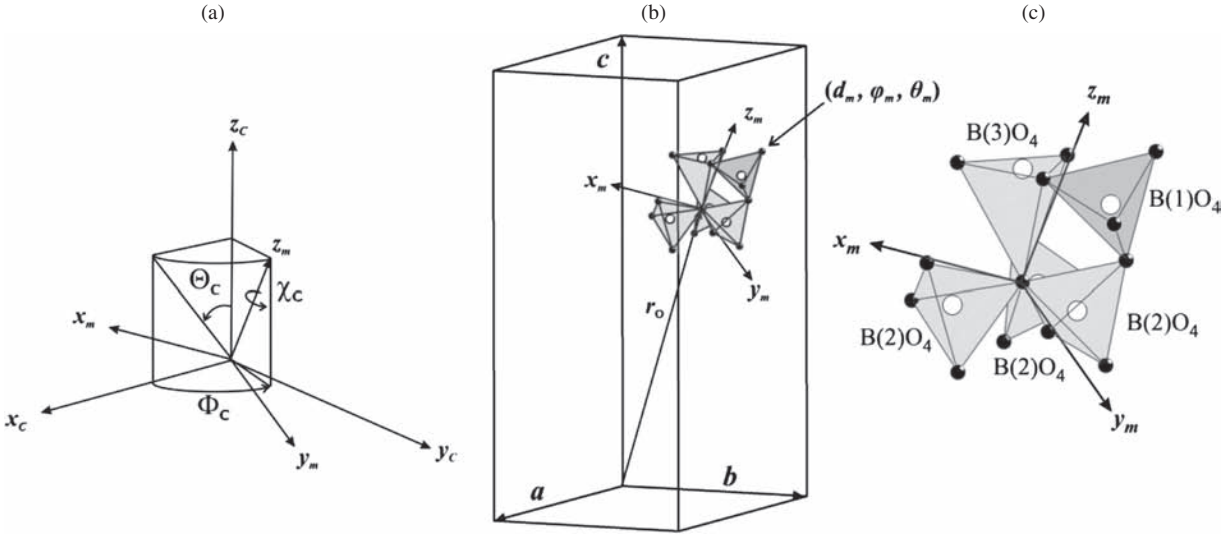

Fig. 1. Rigid body group (RBG) defined for performing the Rietveld refinement of the XRD pattern of the $Fe_{1.5}Zn_{1.5}B_7O_{13}Cl$ mixed boracite. (a) Orthogonal coordinate system to perform the rotations of the RBG: first a rotation χ_C of the whole RBG around the z_m axis is performed (z_m is coincident with z_C at the beginning); next, a rotations of the whole RBG inclining their z_m-axis by the angles Θ_C and Φ_C are applied. (b) A translation of the origin of the RBG to the position r_O is performed. Here, the RBG is represented isolated in the unit cell. The spherical coordinates (d_m, ϕ_m, θ_m) in the (x_m, y_m, z_m) orthogonal coordinate system may be refined or not in the last step of the refinement process. (c) Detailed representation of the RBG in the (x_m, y_m, z_m) coordinate system. The orthogonal (x_C, y_C, z_C) coordinate system is defined in such a way that x_C is coincident with the *a*-axis, y_C is contained in the *ab* plane, and z_C is perpendicular to the *ab* plane. In the Rietveld refinement for the $Fe_{1.5}Zn_{1.5}B_7O_{13}Cl$ mixed boracite, the positional parameters that were refined were χ_C, Θ_C, Φ_C as well as the *z*-coordinate for the origin of the RBG.

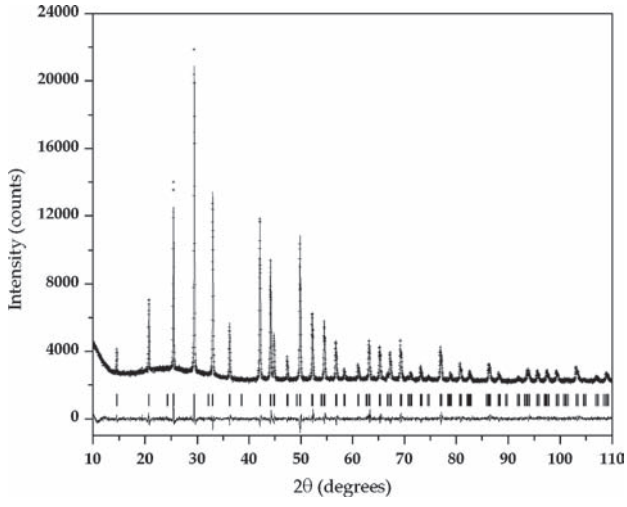

Fig. 2. Observed (crosses), calculated (solid line) and difference (solid line at the bottom) from the final Rietveld refinement of the X-ray powder diffraction data of $Fe_{1.5}Zn_{1.5}B_7O_{13}Cl$ mixed boracite at room temperature. Vertical marks correspond to the positions allowed for the Bragg reflections.

step of refinement the spherical internal coordinates for B(3) and O(2) were refined in such a way to allow to bring the $B(3)O_3$ triangle closer to the O(1) atom. The RBG subroutine has been included in the program FULLPROF.[27]

The use of the RBG reduced significantly the number of positional parameters in the Rietveld refinement. At this stage, the refinement successfully proceeded and ended with sound merit figure values $\chi^2 = 2.25$ and $R_B = 6.12\%$. X-ray diffraction patterns of experimental, calculated and difference are plotted in Figure 2. R-Bragg and R-pattern $R_B = 0.061$ $R_p = 0.022$ are the quality-of-fit parameters for boracite $Zn_{1.5}Fe_{1.5}B_7O_{13}C1$. Since, the R-Bragg depends strongly on the fit of the structure parameters than the other agreement indices and R-pattern is influenced by the intensity of the diffraction line as well as the background. A good estimation of these in $Zn_{1.5}Fe_{1.5}B_7O_{13}C1$ represents a correct adjustment from powder profile refinement with the rigid body formalism employed. These parameters in agreement with previous values of R-pattern and R-Bragg factors reported to $Zn_3B_7O_{13}Cl$ ($Rp = 0.081$ and $R_B = 0.047$)[12] and the R factor widely used in single-crystal structure analysis as in $Fe_3B_7O_{13}Cl$ ($R = 0.081$).[28] The structural parameters determined from X-ray powder diffraction data at room temperature are summarized in Table I.

Table I. Lattice parameters and discrepancy factors for $Fe_{1.5}Zn_{1.5}B_7O_{13}Cl$, space group $R3c$ (No. 161).

Lattice parameters	
a (Å)	8.5726 (1)
c (Å)	21.0116 (4)
Vol. (Å^3)	1337.26 (3)
Reliability factors (%)	
R_P	2.19
R_{exp}	1.93
R_{Bragg}	6.12

Table II. Final refined positional and thermal parameters for $Fe_{1.5}Zn_{1.5}B_7O_{13}Cl$ at room temperature. The crystal symmetry is given by the space group $R3c$ (No. 161).

Atom	X	Y	Z	B (Å^2)
Cl	0	0	0.2667	1.5 (2)
Zn/Fe	0.1438 (7)	0.2964 (2)	0.3226 (2)	0.40 (3)
B(1)	−0.1641 (9)	0.1702 (9)	−0.092 (1)	0.24
B(2)	0.1034 (6)	−0.1019 (3)	−0.0348 (8)	0.24
B(3)	0	0	0.095 (1)	0.24
O(1)	0	0	−0.018 (1)	0.43 (7)
O(2)	−0.0062 (6)	−0.1626 (9)	0.0983 (8)	0.43 (7)
O(3)	0.2927 (8)	0.264 (1)	−0.041 (1)	0.43 (7)
O(4)	0.2017 (4)	−0.0214 (1)	−0.0932 (9)	0.43 (7)
O(5)	0.2284 (6)	−0.0778 (4)	0.0162 (8)	0.43 (7)

Table III. Main bond distances (Å) in the $Fe_{1.5}Zn_{1.5}B_7O_{13}Cl$ mixed boracite at room temperature.

Zn/Fe	Cl	2.495 (2)	B(1)	O(2)	1.561 (1)
	O(2)	2.052 (3)		O(3)	1.520 (3)
	O(3)	2.097 (6)		O(4)	1.42 (2)
	O(4)	2.020 (4)		O(5)	1.42 (4)
	O(5)	2.060 (6)			
			B(2)	O(1)	1.565 (5)
B(3)	O(2)	1.37 (4)		O(3)	1.46 (4)
	O(1)	2.374 (1)		O(4)	1.45 (2)
				O(5)	1.455 (1)

Final refined positional and thermal parameters are given in Table II, and the main interatomic distances are given in Table III.

The unit cell for the $Fe_{1.5}Zn_{1.5}B_7O_{13}Cl$ mixed boracite is shown in Figure 3.

The cell parameters for the $Fe_{1.5}Zn_{1.5}B_7O_{13}Cl$ boracite, are almost the average value between those reported for $Fe_3B_7O_{13}Cl$ (ICSD 60504)[28] and $Zn_3B_7O_{13}Cl$ (ICSD 55444);[12] which are in good agreement with a 50–50% composition of Fe–Zn in the mixed boracite subject of this paper. The effect of include Fe in the structure is to increase the a, c unit-cell parameters and cell volume in 1, 0.4 and 2.5% respectively as a consequence of the slightly major size of the ionic radius for Fe.

On the other hand, bond valence calculations were made using the recommended bond-valence parameters for oxides published by Brese & O'Keeffe[29] and considering those coordination polyhedra whose bond valence calculations were based on distances and angles that were allowed to refine (this was partially true in some cases). For the B(3) atom, the contribution of the fourth oxygen atom O(1) to the bond valence sum obtained for the $B(3)O_3$ triangle of 3.01 is increased to 3.07 (i.e., only 0.06 v. u. indicating the presence of avery weak bond in the

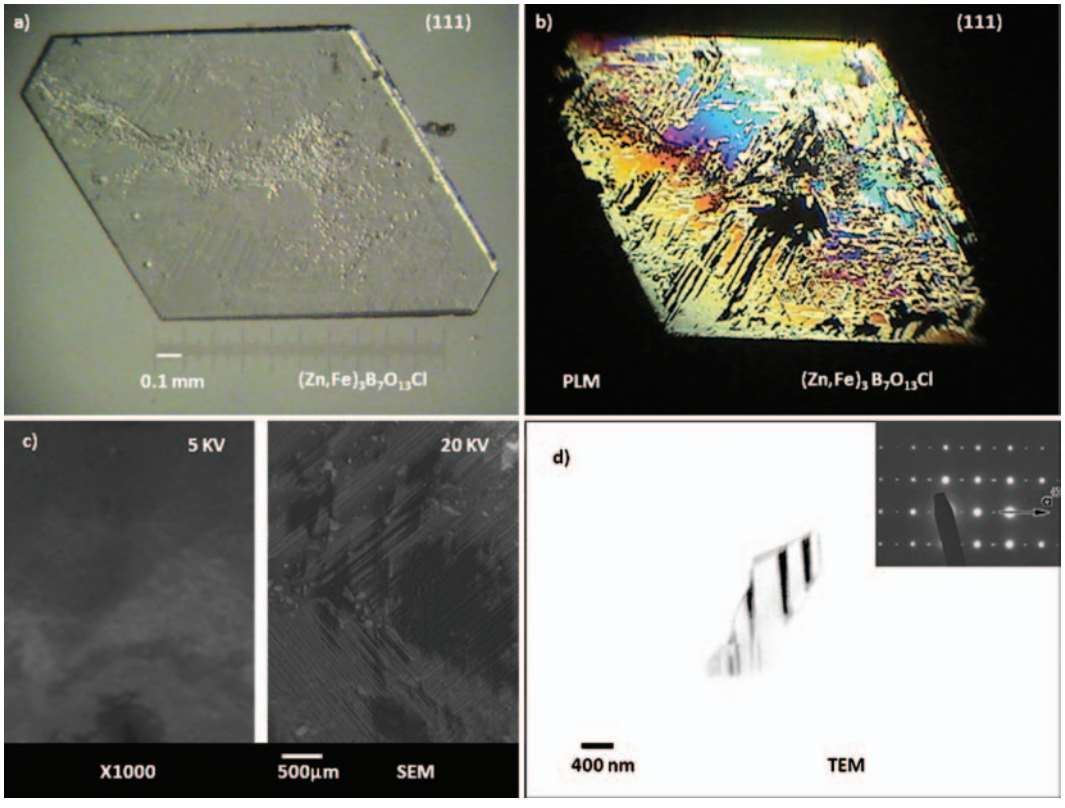

Fig. 4. (a) Platelet cut and polished from as-grown crystal parallel to a naturally formed (111) facet for $Fe_{1.5}Zn_{1.5}B_7O_{13}Cl$ for PLM and SEM measurements. (b) The PLM image shows strongly birefringent lamellae oriented approximately along [100]. (c) Microdomain structure as observed by SEM. The microdomain structures are parallel to (100). (d) TEM bright-field image of spike-like nanodomains are oriented along (100) in $Fe_{1.5}Zn_{1.5}B_7O_{13}Cl$ boracite. The incident electron beam is closely parallel to [001].

right position for have a distorted tetrahedral coordination around the planar triangle coordination for the third boron atom B(3). This fact is also a feature for the reported boracites $Fe_3B_7O_{13}Cl$ (ICSD 60504),[28] $Zn_3B_7O_{13}Cl$ (ICSD 55444)[12] and recently $Fe_{1.59}$ $Zn_{1.41}B_7O_{13}Br$.[30] These results supports the refined model obtained for the crystal structure of the $Fe_{1.5}Zn_{1.5}B_7O_{13}Cl$ boracite by using the rigid body formalism in dealing with the case of boron atoms with very low scatter power for X-rays.

3.2. Domain Structure

As-grown single crystals of boracites often display beautiful large domains; however, a great number of them show complicated lamellar configurations. The domain structure in the trigonal phase of $Fe_{1.5}Zn_{1.5}B_7O_{13}Cl$ is observed along the [111] pseudocubic direction (see Fig. 4(b)), since the polarization vector, P_s, in the trigonal phase lies along a pseudocubic [111] direction,[31] however the domains becomes present in the parallel cut sections to the planes pseudocubic {100}, {110} and {111}.[31] Schmid has determined that a domain with four possible orientations in the trigonal phase always has the same configuration formed by its electric dipole direction.[31] Under the polarizing microscope, it is possible to identify the domains present in $Fe_{1.5}Zn_{1.5}B_7O_{13}Cl$ as 180° head–head or tail–tail domains. No explanation for their presence exists to date, although their origin could be related to growth stacking faults.[32]

Concerning the application of a SEM for revealing the domain structure in ferroelectric materials, Le Bihan has developed a theoretical model of the charging mechanism of an insulating sample irradiated by an electron beam.[33] According to such a model at accelerating voltages, V_{acc}, of a few kV an equilibrium of the electron currents impinging on the surface of the sample and leaving it can be obtained and the specimen does not charge up, thus allowing domains in ferroelectric crystals to be observed. The equilibrium voltage (V_o in Le Bihan's study) depends on the material under observation, as well as some other parameters. When observing domains in ferroelectric crystals, Maussion and Le Bihan[31] have shown that positive ends of domains appear dark compared to negative ones. This contrast is due to the potential difference between domains of opposite polarity induced by spontaneous polarization. Although we have not experimentally correlated the polarity of domains in our samples, it is evident that secondary electrons are attracted by positive domains (dark contrast) or rejected by negative domains (light contrast). After PLM observations, the

same non-metallised, non-etched $Fe_{1.5}Zn_{1.5}B_7O_{13}Cl$ sample was examined with the SEM, where the pressure was $5 * 10^{-6}$ mbar, in secondary electron emission mode. In our experiment, the application of an accelerating voltage of 5.0 kV to $Fe_{1.5}Zn_{1.5}B_7O_{13}Cl$ samples was not enough to revealing the domain structure (see Fig. 4(c)). We needed to apply 20 kV (see Fig. 4(c)). This equilibrium voltage is different in value to those used for revealing the domain structure by SEM in other boracites ($Mn_3B_7O_{13}I$ $V_{acc} =$ 10 kV and $Zn_3B_7O_{13}X$ $V_{acc} = 5$ kV).[6, 8]

Using TEM in bright field mode, we can identify nano-domain structures, Figure 4(d). The examination by TEM showed that in the trigonal/rombohedral system of $Fe_{1.5}Zn_{1.5}B_7O_{13}Cl$ domain structures exist. Thin (50–100 nm) mostly planar domains parallel to (100) were frequently observed in $Fe_{1.5}Zn_{1.5}B_7O_{13}Cl$ boracite (Fig. 4(d)). They can be explained as twin lamellae with (100) as the twin plane in the trigonal (R3c) symmetry. The observed domains could be considered as ferroelectrics and they could be created by the trigonal/rombohedral distortion. However a more detailed discussion on the nature of the domains will be presented in future works.

4. CONCLUDING REMARKS

Single crystals of $Fe_{1.5}Zn_{1.5}B_7O_{13}Cl$ boracite were grown by chemical transport reactions in closed quartz ampoules, at a temperature of 1173 K and were examined by polarizing optical microscopy (PLM), scanning electron microscopy (SEM) and transmission electron microscopy (TEM). For both PLM and SEM, the same as-grown samples were used without having to resort to metallization of the crystal faces. For TEM the single crystals were crushed and mounted on holey carbon films. Comparative electron microscope images were useful for revealing the nano and micro domain structure of this material previously observed between the crossed polars of an optical microscope. X-ray diffraction analysis of the pulverized crystals was performed. The compound crystallizes in the trigonal/rombohedral system with cell parameters $a = 8.5726(1)$ Å, $c = 21.0116(4)$ Å, $V = 1337.26(3)$ Å^3, $Z = 6$ and space group $R3c$ (No. 161).

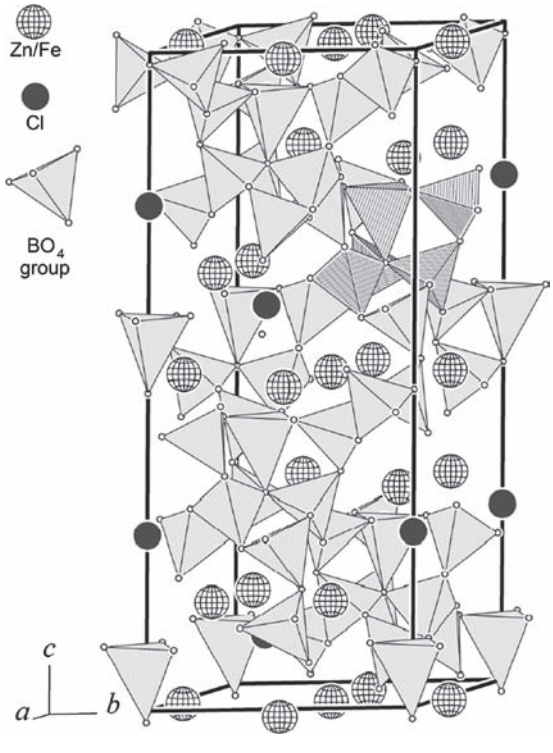

Fig. 3. Representation of the unit cell for the $Fe_{1.5}Zn_{1.5}B_7O_{13}Cl$ mixed boracite.

Acknowledgments: The authors thank José Carlos Carballo-Bastida from Cicese-Ensenada, Mexico for his valuable technical support. I. Rosales acknowledges the fellowship of CONACyT for supporting her postdoctoral programme.

References and Notes

1. J. D. Dana, Dana's System of Mineralogy, edited by C. Palache, H. Berman, and C. Frondel, John Wiley Press, New York **(1951)**.
2. W. G. Hankel, Ueber die Thermoelektrischen Eigenschaften des Boracites. Abhandlungen der Matematisch-Physischen Classe, Der Koeniglich Saechsischen, Gesellschaft der Wissenschaften, edited by S. Hirtzel, Leipzig **(1859)**, Vol. 4.
3. R. M. Honea and F. R. Beck, *Am. Mineralogist* 47, 665 **(1962)**.
4. J. D. Dana, New Mineralogy, 8th edn., edited by R. V. Gaines, H. Catherine, W. Skinner, E. E. Foord, B. Mason, and A. Rosenzweig, John Wiley Inc., New York **(1997)**, pp. 25.5–25.6.
5. H. Schmid, *J. Phys.: Condens. Matter* 20, 434201 **(2008)**.
6. A. G. Castellanos-Guzman, J. Campa-Molina, and J. Reyes-Gomez, *J. Microscopy* 185, 1 **(1997)**.
7. J. Campa-Molina, S. Ulloa-Godínez, A. Barrera, L. Bucio, and J. Mata, *J. Phys.: Condens. Matter* 18, 4827 **(2006)**.
8. J. Campa-Molina, O. Blanco, A. Correa-Gomez, M. Czank, and G. A. Castellanos-Guzman, *Journal of Microscopy* 208, 201 **(2002)**.
9. K. Aizu, *Phys. Rev. B* 2, 754 **(1970)**.
10. H. Schmid, Ferroelectric Ceramics, edited by N. Setter **(1992)**, p. 107.
11. H. Schmid and H. Tippmann, *Ferroelectrics* 20, 21 **(1978)**.
12. S. Y. Mao, M. E. Mendoza-Alvarez, W. Depmeier, F. Kubel, and H. Schmid, *Ferroelectrics* 115, 91 **(1991)**.
13. V. K. Wadhawan, Introduction to Ferroic Materials, Gordon and Breach Scientific Publications, Amsterdam **(2000)**, pp. 189–215.
14. E. H. K. Salje, Phase Transitions in Ferroelastic and Coelastic Crystals, Cambridge University Press, Cambridge **(1993)**, pp. 1–8.
15. J. Fousek, Ferroelectric Ceramics, edited by N. Setter **(1992)**, Vol. 16, p. 87.
16. V. K. Wadhawan, *Phase Transitions* 64, 165 **(1998)**.
17. W. Cao and L. E. Cross, *Ferroelectrics* 157, 19 **(1994)**.
18. H. Schmid and J. Schwarzmueller, *Ferroelectrics* 10, 283 **(1976)**.
19. E. Burzo, Boracites Me3B7O13X and related compounds, Landolt-Börnstein Numerical Data and Functional Relationships in Science and Technology, New Series Group III. 27h, Springer-Verlag, Berlin **(1993)**, pp. 128–204.
20. L. Smart and E. Moore, Solid State Chemistry, An Introduction, Chapman and Hall, London **(1992)**.

21. S. Mathews, R. Ramesh, T. Venkatesan, and J. Benedetto, *Science* 276, 238 **(1997)**.
22. J. Campa-Molina and A. G. Castellanos-Guzman, *Solid State Commun.* 89, 963 **(1994)**.
23. H. Schmid, *J. Phys. Chem. Solids* 26, 973 **(1965)**.
24. M. Schindler and F. C. Hawthorne, *Canadian Mineralogist* 36, 1195 **(1998)**.
25. J. Rodríguez-Carvajal, D. B. Wiles, and R. A. Young *J. Appl. Crystallogr.* 14, 149 **(1981)**.
26. P. Thompson, D. E. Cox, and J. B. Hastings, *J. Appl. Crystallogr.* 20, 79 **(1987)**.
27. V. Rodríguez and J. Rodríguez-Carvajal, Guide for the General Rigid Body Constraints/TLS Subroutine for Rietveld Refinements, Short Reference Guide of the program Fullprof **(1997)**, http://www.ill.eu/sites/fullprof/php/reference.html.
28. M. E. Mendoza-Alvarez, K. Yvon, W. Depmeier, and H. Schmid, *Acta Crystallographica C* 41, 1551 **(1985)**.
29. N. E. Brese and O'Keeffe, *Acta Cryst. B* 47, 192 **(1991)**.
30. S. Ulloa-Godínez, I. Rosales, L. Bucio, M. H. Farías, and J. Campa-Molina, *Acta Cryst.* E65, i83 **(2009)**.
31. H. Schmid, *Growth Crystals* 7, 25 **(1969)**.
32. H. Schmid, *Phys. Stat. Sol*. 37, 209 **(1970)**.
33. R. Le Bihan, *Ferroelectrics* 97, 19 **(1989)**.

Received: 11 November 2009. Accepted: 8 April 2010.